

High resolution spaceborne INSAR simulation with extended scenes

K. ELDHUSET

Norwegian Defence Research Establishment (FFI)

Abstract. The Inverse-EETF4 (Extended Exact Transfer Function 4th order) is used to simulate raw data and a complete INSAR processing chain for high squint has been developed. Phase differences for a spaceborne INSAR geometry are estimated and used as input to the Inverse-EETF4 and then the simulated raw data are processed with EETF4. The standard deviation of the flattened interferogram is only a few degrees. The Inverse-EETF4 is used to simulate extended SAR raw data from IKONOS images. The standard deviation of the auto-interferogram generated from those data is a few tenths of a degree. The simulations have been done with squint up to 40° , range block size of 1100 pixels and spatial resolution around 0.3 m. The Inverse-EETF4 and EETF4 processing is performed by generation of discontinuous raw data which makes it possible to cope with very large range migration.

1. Introduction

The EETF (Extended Exact Transfer Function) (Eldhuset 1998) is an algorithm which was developed optimized for spaceborne SAR (Synthetic Aperture Radar) processing. The approximations done in EETF4 must be found in Eldhuset (1998) and in Eldhuset (2003a) for EETF2. It is shown in Eldhuset (2003b and 2001) that the spaceborne formalism which the EETF4 is based upon is necessary in order to represent the azimuth phase history with sufficient accuracy for some squint and spatial resolution less than 1 m for X-band. Furthermore, the multi-block processing approach in the EETF4 is necessary to cope with high Doppler centroid variations over the swath for a squinted spaceborne SAR. The examples in this paper are for cases when the azimuth phase history used in the airborne formalism is not sufficient.

A spotlight raw data simulator for extended scenes was for the first time published in Cimmino (2003) where the focus depth variation is taken care of for a nonsquinted geometry and a straight line flight path. Here, a unique INSAR (Interferometric SAR) raw data simulator for extended scenes with very high resolution using the Inverse-EETF4 is developed. The space-variance of the SAR transfer function is handled in the same way as in the EETF4 for a squinted SAR and a very long synthetic aperture of a curved orbit. The

Inverse–EETF4 simulates raw data for extended targets for a squinted SAR in a very efficient way by using multi–block processing and representing the enormous range migration in very compact way. The main modules of the INSAR simulation chain will be described in §2. The phase quality is measured in a flattened interferogram processed with the INSAR simulator including the Inverse–EETF4 and the EETF4. Finally, in §3 it is shown how INSAR raw data for extended targets can be generated by using IKONOS data as input to the Inverse–EETF4. The phase quality is measured from an auto–interferogram generated from those raw data.

2. INSAR simulation

The INSAR simulation chain consists of five main steps which are listed below.

1. Estimation of Doppler parameters with a given Kepler orbit, squint angle and look angle.
2. Estimation of phase differences from an earth ellipsoid (all types of orbit).
3. Estimation of an INSAR raw data pair using Inverse–EETF4.
4. Processing of two SLCs (Single Look Complex) from two raw data sets using EETF4.
5. Interferogram generation (‘flattening’ to an ellipsoid)

The flow diagram of the INSAR simulation is shown in figure 1. The SAR system parameters used for the simulation are given in table 1 and the Kepler elements are given in table 2.

2.1 *Doppler parameter estimation*

The Doppler parameter estimation module provides Doppler parameters to the two Inverse–EETF4 modules and to the two EETF4 modules as shown in figure 1. The Doppler parameters are estimated as described in Eldhuset (1998) and the four Doppler parameters used here are given in tables 3 and 4 for a low squint case and a high squint case, respectively.

2.2 *Simulation of phase differences*

Figure 1 shows that two Inverse–EETF4 modules are used to simulate two raw data sets. One of the Inverse–EETF4 modules takes as input an image with both constant amplitude

and phase. The other Inverse–EETF4 module takes the phase difference image. Figure 2 shows the principle for phase difference estimation. The phase difference of the distances from the two orbits O_1 and O_2 to the target point T on the ellipsoid is given by

$$\Delta\phi = 4\pi \frac{R_2 - R_1}{\lambda} \quad (1)$$

where λ is the radar wavelength. \vec{Z} is the z -axis of the local relative reference frame which is perpendicular to the earth ellipsoid. The horizontal distance between the satellite orbits O_1 and O_2 which we call the effective baseline is given by $B_{x,eff} = B_x/\cos(\text{yaw})$ where B_x is the shortest distance between the orbits. From figure 1 we see that the module called Lookangle–range estimation (see §2.4) provides input to both the Phase difference estimation and to the Interferogram generation modules (see §2.4). Figure 3 shows the phase differences estimated with equation 1 and wrapped between 0 and 2π .

2.3 Inverse–EETF4

In Eldhuset (2001 and 2003b) it is shown that a 4th order phase history can be used in the azimuth reference signal for extremely long apertures and high squint. The azimuth reference signal is an approximation of the Kepler azimuth signal, which we define as the azimuth signal corresponding to the relative motion of a satellite in a Kepler orbit and a rotating ellipsoid earth. For $\text{yaw}=5^\circ$ and 1 foot azimuth resolution it was found that a 4th order signal is sufficient. For $\text{yaw}=40^\circ$ it was found that a 5th order signal is extremely accurate while for a 4th order signal there is a loss in the point target response of only 0.003 dB and the left and right sidelobe differ 0.6 dB. We have therefore used the Inverse–EETF4 for all simulations in this work. However, a fast algorithm could be implemented in 5th order if necessary. If a higher order should be required, a numerical method is needed in the stationary phase approximation to solve an equation with order greater than 5.

The Inverse–EETF4 flow diagram is very similar to the EETF4 flow diagram in Eldhuset (1998). The Inverse–EETF4 starts with an input image that can in principle be the complex reflectivity pattern of an imaged surface and the output is the complex raw data. A scattering theory based on Maxwell’s equations and using Green’s function and Kirchhoff approach for calculation of the reflectivity pattern can be found in Franceschetti *et al.* (2002). A revised scattering theory for ultra high resolution has been development at FFI and may in the future be the input to the Inverse–EETF4. In this work we use either

(constant amplitude, constant phase), (varying amplitude, constant phase) or (constant amplitude, varying phase). The main filter of the EETF4 is denoted $H_{EETF4}^*(\omega_r, \omega_a; R_m)$ (Eldhuset (1998)) and of the Inverse-EETF4 in figure 4 it is $H_{EETF4}(\omega_r, \omega_a; R_m)$, where (ω_r, ω_a) are the range and azimuth frequencies. In the EETF4 the phase correction is denoted $\Delta\Phi_{EETF4}(\omega_a; R, R_m)$ and in the Inverse-EETF4 it is $-\Delta\Phi_{EETF4}(\omega_a; R, R_m)$, as shown in figure 4. We note that the main filter $H_{EETF4}(\omega_r, \omega_a; R_m)$ is dependent on the Doppler parameters in the center of the block and can be written in the following way

$$H_{EETF4}(\omega_r, \omega_a; R_m) = H_{EETF4}\{\omega_r, \omega_a; a_1(R_m), a_2(R_m), a_3(R_m), a_4(R_m)\} \quad (2)$$

where R_m is the slant range in the center of a block and the four Doppler parameters are dependent on slant range as indicated in equation 2. The center of a block corresponds to the center of a range compressed block. The phase correction $-\Delta\Phi_{EETF4}(\omega_a; R, R_m)$ is dependent on the Doppler parameters in the center of the block at slant range R_m and on the Doppler parameters at range R in the block, and can be written

$$-\Delta\Phi_{EETF4}(\omega_a; R, R_m) = -\Delta\Phi_{EETF4}\{\omega_a; a_1(R), a_1(R_m); a_2(R), a_2(R_m); a_3(R), a_3(R_m); a_4(R), a_4(R_m)\} \quad (3)$$

The phase correction in equation 3 is applied in each azimuth line corresponding to slant range R after forward azimuth FFT as shown in figure 4. The number of samples of the filter in the frequency domain in azimuth and range can be found by

$$N_{az} = N_{FFT,az} \frac{|a_2|T_{az}}{PRF} \quad (4)$$

$$N_{ra} = N_{FFT,ra} \frac{B_{ra}}{f_s} \quad (5)$$

where we use $N_{FFT,az} = 2^{17} = 131072$ when the azimuth resolution is about 0.3 m and $N_{FFT,ra} = 2^{11} = 2048$. From table 1 we see that $PRF = 27780\text{Hz}$, the integration time is $T_{az} = 4.7\text{s}$, the range sampling frequency is $f_s = 610\text{MHz}$ and the range chirp bandwidth is $B_{ra} = 500\text{MHz}$. From table 3 the azimuth Doppler rate is $|a_2| = 5143.0\text{Hz/s}$. Using equations 4 and 5 yields $N_{az} = 114049$ and $N_{ra} = 1678$. Now we estimate the size of the matrices which corresponds approximately to the virtual memory needed for the Inverse-EETF4. Two matrices with 131072×2048 complex samples (8 bytes for each sample) are needed. The size of the matrices is then $131072 \times 2048 \times 8 \times 2 = 4.3\text{GBytes}$. The programs were compiled with FORTRAN 90 and run on an HP 9000 N-4000-36 computer with 8

GBytes physical memory. The two Inverse–EETF4 programs were run in parallel on two CPUs followed by the two EETF4 programs in parallel for generation of two SLC data sets.

If the resolution is very good and the squint is very high the range cell migration may be thousands of pixels. Figure 5 shows what we will denote continuous and discontinuous raw data in the time domain both in azimuth and range. In the left figure the raw data of a point target P is continuous. In the right figure the same raw data is split into two parts P1 and P2 where the matrix is half of the size in range. If there is very large range cell migration, the point target P may be split in n partial point targets (P1...Pn) and the size of the matrix is reduced a factor n. If the Doppler centroid is around 200000 Hz (yaw=40°) as in table 4 the range cell migration is 54000 pixels when $f_s = 610 \text{ MHz}$, $N_{az} = 114049$ and $PRF = 27780$. We would need a matrix of size 131072 pixels in azimuth (see above) and $N_{FFT,ra} = 2^{16} = 65536$ pixels in range. Simulation of continuous raw data with the EETF4 requires about 137 GB. If we instead simulate discontinuous raw data we need 4.3 GB, which means a memory saving factor of 32 compared to simulation of continuous raw data. We see that we don't need larger matrices for the raw data in the time domain than in the frequency domain.

As mentioned the Inverse–EETF4 algorithm can also do multi–block processing. The input image in figure 4 can be divided into several sub images (blocks) and the raw data of each block are processed. Finally the complex raw data of each block are added coherently. For multi–block inverse processing one more matrix is needed where the raw data from each block are summed coherently. This gives us the possibility to simulate the raw data closer to a time domain raw data generation. This may be especially important for a space-borne SAR with large squint where the Doppler centroid changes a lot over range. In this way we can simulate the raw data with the Inverse–EETF4 using small blocks and achieve the quality of raw data as close to time domain processing as we want, however, much faster. Then we can process with EETF4 using much larger blocks. For a given SAR we can determine the maximum block size allowed for the EETF4 processing if we have defined the image quality requirements. At 0.3 m spatial resolution we had to process with only one block in the Inverse–EETF4 due to memory limitations. In Eldhuset (2001 and 2003b) we investigated what happened with increasing squint and Doppler centroid variation by processing small blocks with the Inverse–EETF4 and larger blocks with EETF4

with worse resolution than here. Analysis with 1 m resolution showed that a small mislocation of the impulse responses was present at squint $12\text{--}15^\circ$ using two blocks in the Inverse-EETF4 and one block of size 565 pixels in range in the EETF4. In table 3 we see that the Doppler centroid variation over a swath covering 0.2° in range is 2.05 Hz when the yaw angle is 2° and in table 4 the Doppler centroid changes 805.3 Hz when yaw is 40° . More work should be done to investigate the phase properties of the multi-block processing with the Inverse-EETF4 and the EETF4 at 1 foot resolution.

2.4. Generation of interferogram

The algorithm for generation of an interferogram is described in detail in (Eldhuset *et al.* 2003b) where it was demonstrated for tandem ERS data. The two SLCs are denoted SLC-A and SLC-B in the flow diagram in figure 1. We see also that the Interferogram generation module has input from a table of the look angles associated with slant range as a function of azimuth distance. This table is generated by the module called Lookangle range estimation in figure 1. Figure 6 shows a flattened interferogram with low squint where the yaw angle is 2° . The flattened interferogram in figure 6 corresponds to the input fringe pattern shown in Figure 3. We also processed a flattened interferogram with yaw 40° . We estimated the phase standard deviation for the two images in a region of 400×380 pixels. The standard deviations were 1.08° and 4.9° , respectively. The standard deviation when the yaw angle was 20° was 2.1° . These numbers measure the quality of the whole INSAR simulation chain shown in Fig. 1 with slant range resolution and azimuth resolution around 0.3 m. Further investigation of the phase properties should be done using multi-block processing.

3. Processing of extended targets and auto-interferogram generation

The Inverse-EETF4 can be used to simulate raw data with extended targets. Here we demonstrate that it works with an IKONOS image. The spatial resolution in the image is 1 m, however, this is not assumed in Inverse-EETF4. We assume that the sampling frequency in azimuth is equal to the PRF and in range equal to the range sampling frequency. In figure 7 is shown the image processed with Inverse-EETF4 and EETF4. Compared to the original image it is weakly lowpass filtered. The actual lowpass filter is the Inverse-EETF4 followed by the EETF4. We generated raw data by using the IKONOS image as input to the Inverse-EETF4 (phase=constant, varying amplitude=amplitude in IKONOS

image). Then we processed two SLC images with the EETF4, the second image with an offset in azimuth and range in the raw data. Then an auto-interferogram was generated by taking the phase difference in the overlapping region of the two processed images. The auto-interferogram is shown in figure 8. We processed this image with yaw = 20°, resolution 0.6 m and the offset in azimuth and range was 100 pixels. The phase standard deviation was 1.04° and the mean was 0.55°. We can see the white stripes on the airport very faintly. With yaw = 5° and offset 10 pixels the standard deviation was only 0.19° and the mean was 0.16°. The auto-interferogram corresponds to the standard offset test where the requirement on the standard deviation is a few degrees for real data such as ERS-1/2.

4. Conclusions

A full high resolution INSAR simulation for extended targets has been developed using Inverse-EETF4 and the EETF4. The standard deviation of a flattened interferogram was only a few degrees. IKONOS image data were used as input to the Inverse-EETF4 for simulation of raw data of extended targets. Two SLC data sets were processed with an offset in azimuth and range for auto-interferogram generation. The standard deviation was only a few tenths of a degree. Data with a squint of 40°, resolution 0.3 m and satellite height 500 km were processed. This was possible by using discontinuous raw data, which is a very compact representation of the enormous range migration.

Acknowledgement

This work was supported by FFI and was partly carried out under the WEAG (Western European Armaments Group) EUCLID (European Cooperation for the Long-term In Defence) programs, RTP (Research and Technology Project) 9.8 of CEPA 9.

References

CIMMINO, S., FRANCESCHETTI, G., IODICE, A., RICCIO, D., RUELLO, G., 2003, Efficient Spotlight SAR Raw Signal Simulation of Extended Scenes. *IEEE Transactions on Geoscience and Remote Sensing*, **41**, 2329–2337.

ELDHUSET, K., 1998, A new fourth order SAR processing algorithm for spaceborne SAR. *IEEE Transactions on Aerospace and Electronic Systems*, **34**, 824–835.

ELDHUSET, K., ANDERSEN, P.H., HAUGE, S., ISAKSSON, E., WEYDAHL, D.J., 2003a, ERS tandem INSAR processing for DEM generation, glacier motion estimation and coherence analysis on Svalbard. *International Journal of Remote Sensing*, **24**, 1415–1437.

ELDHUSET, K., 2003b, Ultra High Resolution Spaceborne SAR Processing. *IEEE Transactions on Aerospace and Electronic Systems*, **40**, January 2004.

ELDHUSET, K., 2001, Ultra high Resolution spaceborne SAR processing with EETF4. *Proceedings of the International Geoscience and Remote Sensing Symposium (IGARSS'2001)*, Sydney, 9–13 July 2001 (Piscataway: IEEE/GRSS), CDROM.

FRANCESCHETTI, G., IODICE, A., RICCIO, D., 2002, A Canonical Problem in Electromagnetic Backscattering From Buildings. *IEEE Transactions on Geoscience and Remote Sensing*, **40**, 1787–1801.

Figure 1 Flow diagram for the INSAR simulator.

Figure 2 Geometry for phase difference estimation. Note that the three points O_1 , O_2 and T are in the same plane.

Figure 3 Simulated fringe pattern. The skewed fringes are caused by non-parallel orbits. $Yaw = 40^\circ$.

Figure 4 Flow diagram for Inverse-EETF4 algorithm.

Figure 5 Continuous raw data (P) and discontinuous raw data (P1,P2) of a point target.

Figure 6 Flattened interferogram for INSAR simulation for the data set in Table 3 with $yaw = 2^\circ$. The size of the image is 400 pixels in range and 380 pixels in azimuth.

Figure 7 Inverse-EETF4 and EETF4 using the IKONOS image in Fig. 14 as input with $yaw = 20^\circ$. The spatial resolution in the SAR processor is around 0.3 m since we assume that the sampling frequencies in the IKONOS image are equal to the PRF and the range sampling frequency.

Figure 8 Auto-interferogram using IKONOS image as raw data.

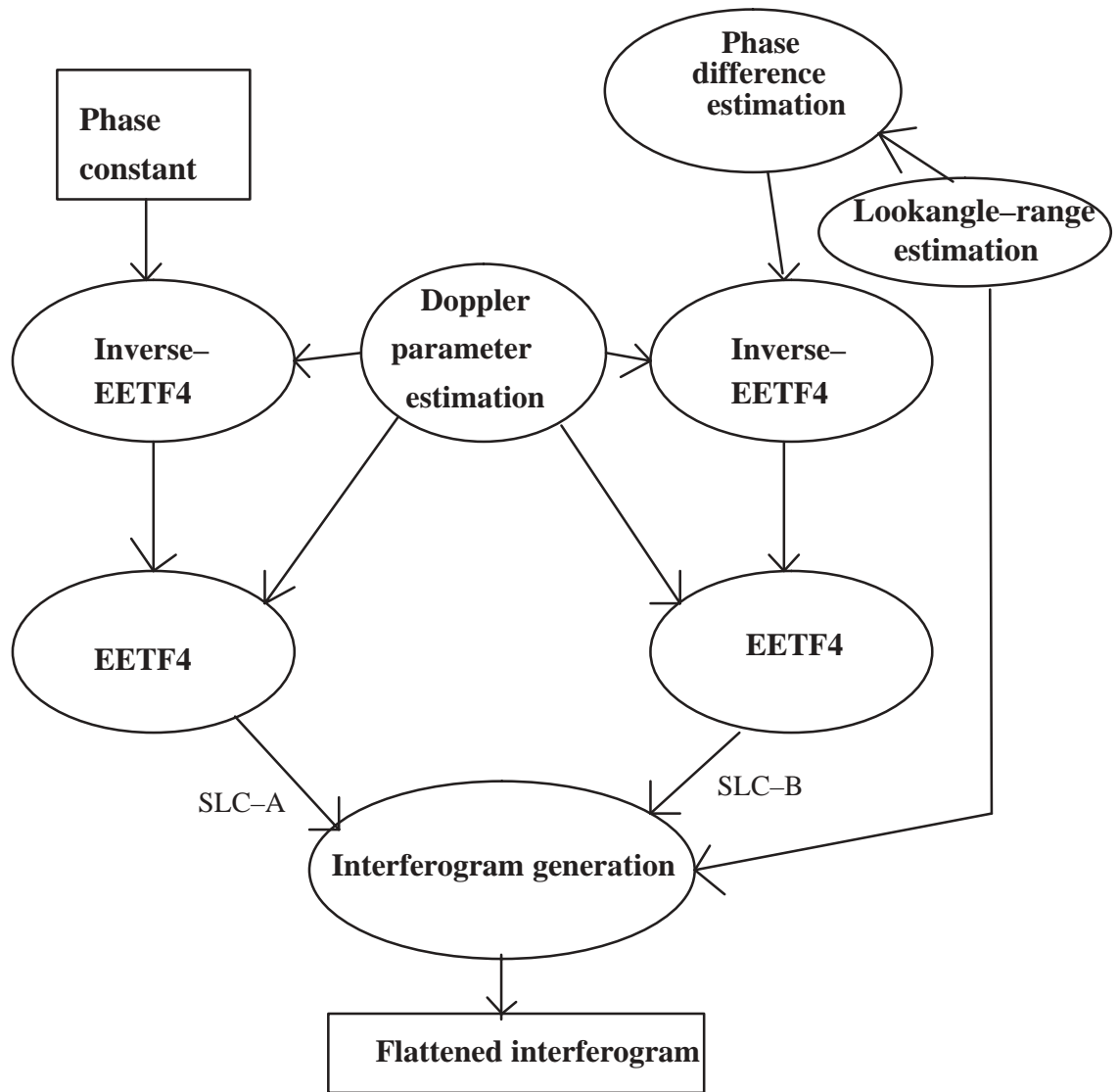


FIGURE 1

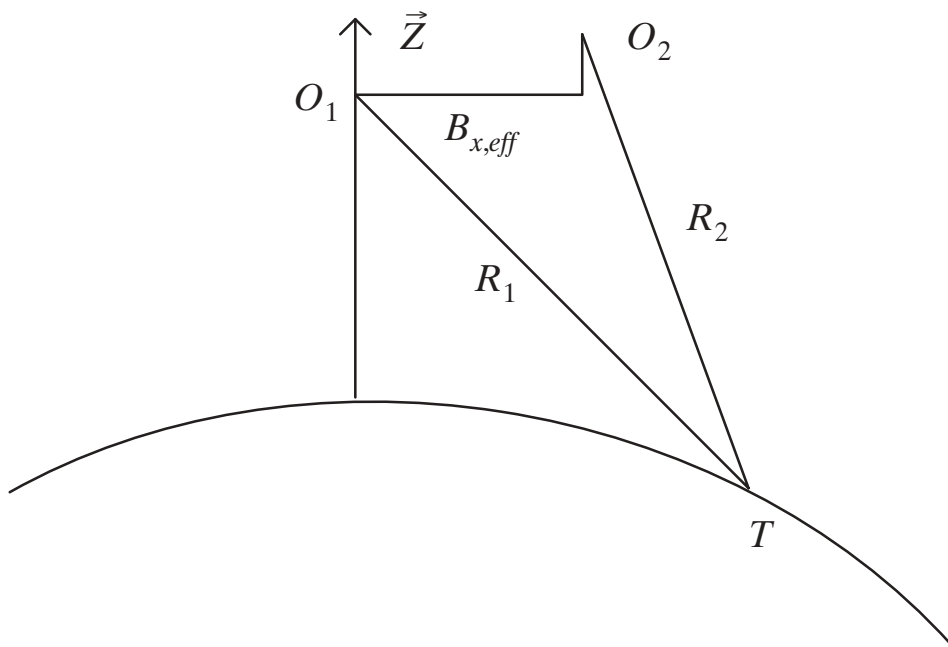


FIGURE 2

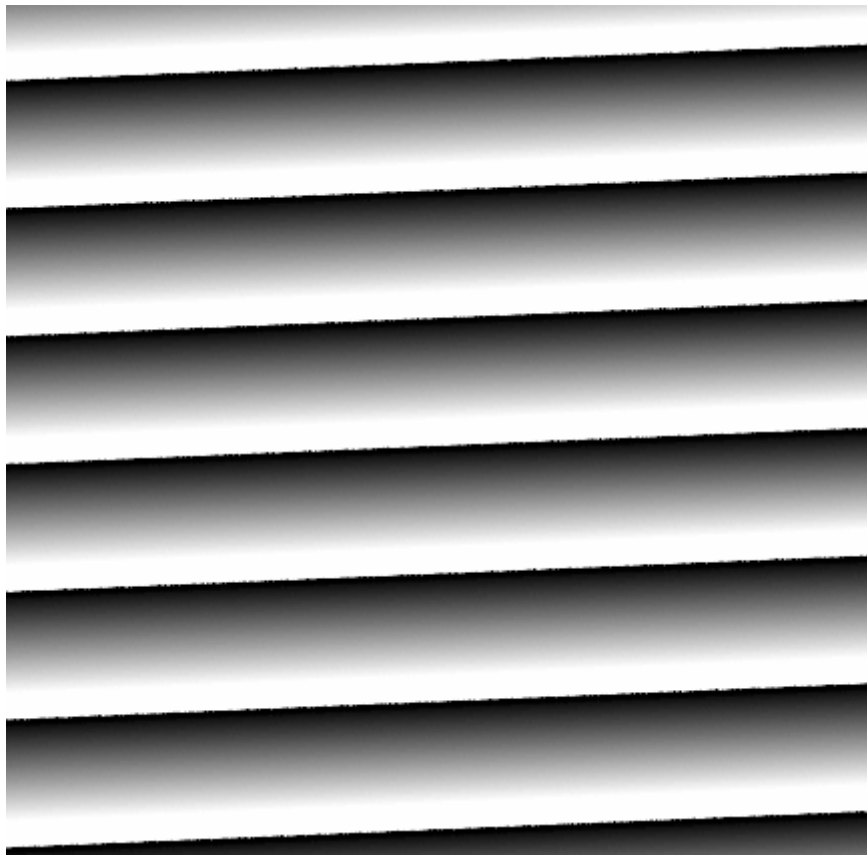


FIGURE 3

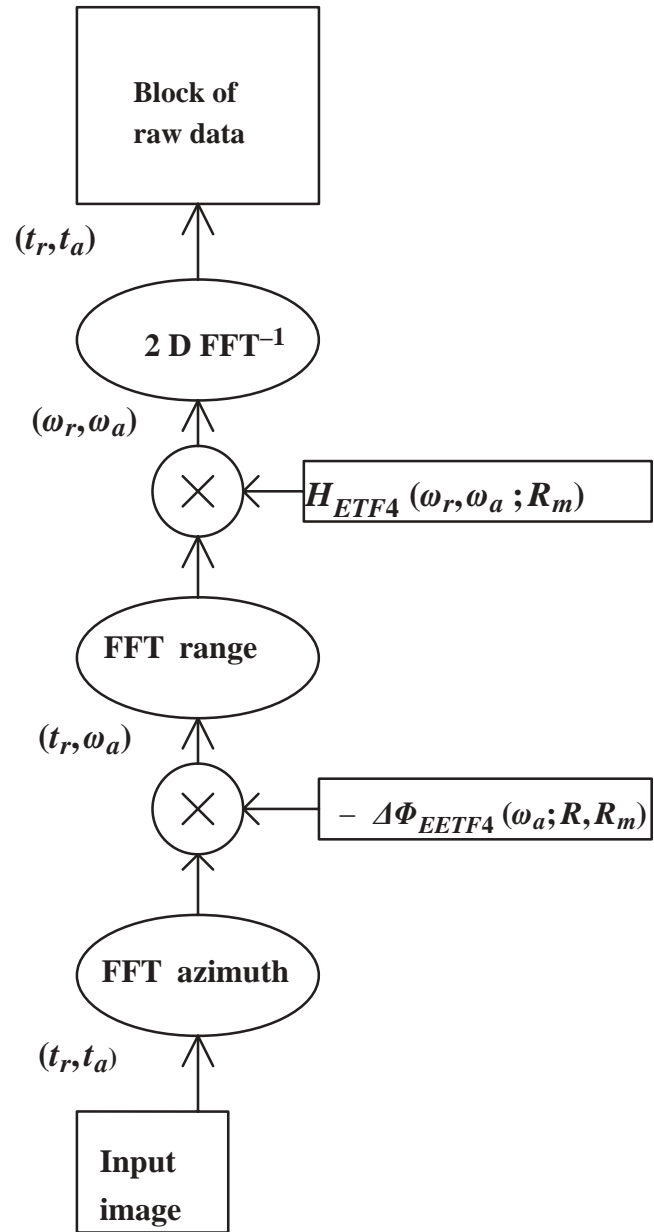


FIGURE 4

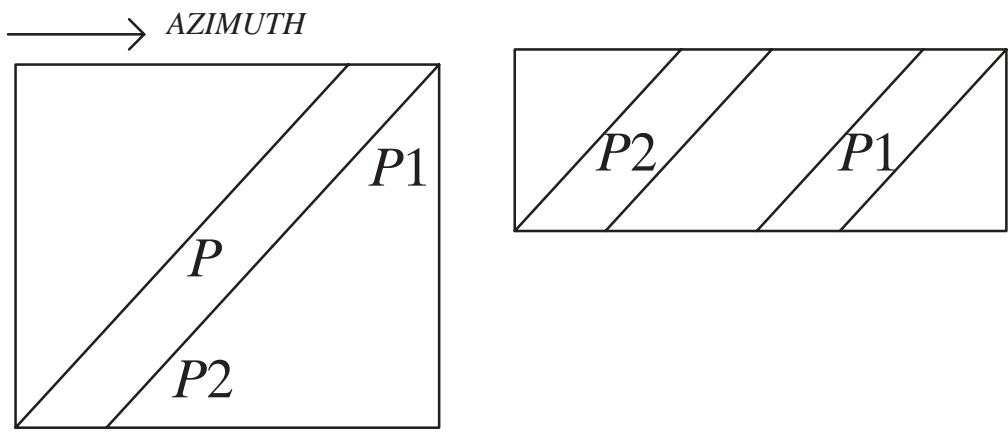


FIGURE 5



FIGURE 6



FIGURE 7

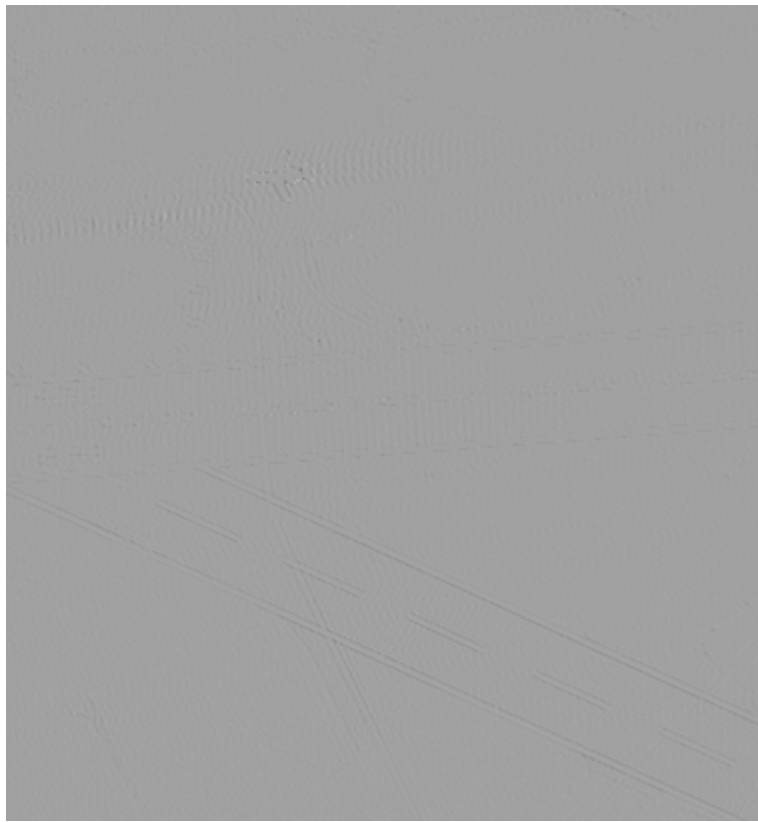


FIGURE 8

Table 1 SAR system parameters for the simulation.

Table 2 The Kepler elements for the selected orbit which has altitude 504219 m at latitude 60° N.

Table 3 Doppler parameters for $yaw = 2^\circ$ at $60^\circ N$ for X-band.

Table 4 Doppler parameters for $yaw = 40^\circ$ at $60^\circ N$ for X-band.

TABLE 1

RF-center frequency	9.6 GHz
Range chirp bandwidth	500 MHz
Range chirp duration	1.25 μ s
Sampling frequency	610 MHz
Integration time	4.70 s
Pulse repetition frequency	27780 Hz

TABLE 2

Semimajor axis (m)	6867000.0
Inclination ($^{\circ}$)	98.0
Eccentricity	0.001
Argument of perigee ($^{\circ}$)	90.0
Altitude at ascending node (m)	498841.9
Altitude at perigeum (m)	506044.5

TABLE 3

Look angle ($^{\circ}$)	Range (m)	a_1 (s^{-1})	a_2 (s^{-2})	a_3 (s^{-3})	a_4 (s^{-4})
39.85	675904.2	-394.90	-5142.90	0.098966	0.308765
40.05	678151.6	-392.85	-5125.39	0.098133	0.305686

TABLE 4

Look angle ($^{\circ}$)	Range (m)	a_1 (s^{-1})	a_2 (s^{-2})	a_3 (s^{-3})	a_4 (s^{-4})
39.85	675925.7	193889.9	-4282.6	-28.868	0.0415
40.05	678173.5	194695.2	-4260.7	-28.746	0.0392